Science Advances
AAAS

advances.sciencemag.org/cgi/content/full/5/11/eaax0939/DC1

Supplementary Materials for

TiO_2 metasurfaces: From visible planar photonics to photochemistry

Yunkai Wu, Wenhong Yang, Yubin Fan, Qinghai Song*, Shumin Xiao*

*Corresponding author. Email: shumin.xiao@hit.edu.cn (S.X.); qinghai.song@hit.edu.cn (Q.S.)

Published 1 November 2019, *Sci. Adv.* **5**, eaax0939 (2019)
DOI: 10.1126/sciadv.aax0939

This PDF file includes:

Supplementary Text

In the main manuscript, we have developed a new method that can convert the TiO_2 into black TiO_2 while preserving the nanostructures. Based on this technique, we have fabricated TiO_2 based all-dielectric metasurfaces and explored their new functions. With the controllable and reversible transition between TiO_2 and black TiO_2, we have experimentally realized the dynamic color nano-printing and extended the applications of metasurfaces from optics to photo-chemistry. In this supplementary material, we will show the detail information about the fabrication, transition, optical characterization, and the photo-reduction.

Section S1. The deposition and transition of TiO_2 film

In the main manuscript, we have mentioned that the TiO_2 film was deposited onto an ITO-coated glass substrate via electron-beam evaporation. Here we show the detail conditions and the characteristics of TiO_2 film. Basically, the ITO-coated glass substrate was cleaned with acetone, methanol, and DI water in ultrasonic for 15 minutes of each step. Then the substrate was placed into the chamber of electron-beam evaporator (Syskey SKE-A-75) and the base vacuum was pumped to 2×10^{-7} Torr. The deposition rate was controlled at 0.8 Å/s and the film thickness was controlled by the depositing time. The top-view scanning electron microscope (SEM) image of the prepared TiO_2 film (see fig. S1(a)) show that the average grain size is less than 20 nm. The root mean square of surface roughness, measured with microscope (AFM), is only as small as 2 nm in fig. S1 (c). Both of roughness and grain sizes are good enough for applications in TiO_2 metasurfaces. The black line in fig. S1(e) shows the X-ray diffraction spectra of the as-deposited TiO_2 film, where no diffraction peaks can be seen. The curves in fig. S1(f) show the refractive index and light extinction ratio of the as-deposited TiO_2 film. The films show high refractive index and low loss in the visible spectrum. Then we know that the as-deposited film is amorphous TiO_2.

The material properties of as-deposited TiO_2 can be changed with the thermal annealing in air. To test the efforts of thermal annealing, we have deposited the TiO_2 onto a Si substrate and annealed in a silica furnace tube. The samples were annealed at 500 ^oC. When the annealing temperature is increased to 500 ^oC, the peaks are presented with $2\theta\sim25.382$ and $2\theta\sim48.31$. These peaks show that TiO_2 has been converted to the anatase phase with the post-deposition annealing process. The samples have also been further annealed at 900 ^oC, the anatase phase was still well kept (fig. S1(e)).

While the post-deposition annealing process can change the crystal quality, it must be used very carefully. As the top-view SEM images shown in fig. S1(a), the as-deposited TiO_2 film is quite smooth and the grain sizes are quite small. This is quite good to fabricate high quality photonic devices. After the high temperature thermal annealing process, the particle size and grain sizes increase obviously. At 500 ^oC, the gain sizes are even as large as 20 nm (see fig. S1(b)), which is too large for the nanostructures used in our metasurfaces. This is the reason that we use the amorphous TiO_2 in this research. Of course, the TiO_2 can also be annealed at relatively low temperature, which will be studied in near future.

After the deposition of TiO_2 film, we have also converted it to black TiO_2 film with H^+ plasma implantation in inductively coupled plasma etching. The transition process is similar to the main manuscript. After the transition process, we can clearly see in the main manuscript that the color of TiO_2 becomes dark or black. This kind of color change can be clearly seen in the absorption

curves, where the light extinction coefficient increases drastically after the ion implantation. By means of AFM measurement as shown in fig. S1(c) and (d), the roughness average of TiO_2 film before and after 3 min H^+ implantation was 1.07 nm and 1.12 nm respectively, which indicates that the plasma implantation process in this work will not impact the surface morphology dramatically. This is different from the thermal annealing and thus the ion implantation is suitable for the transition between TiO_2 and black TiO_2.

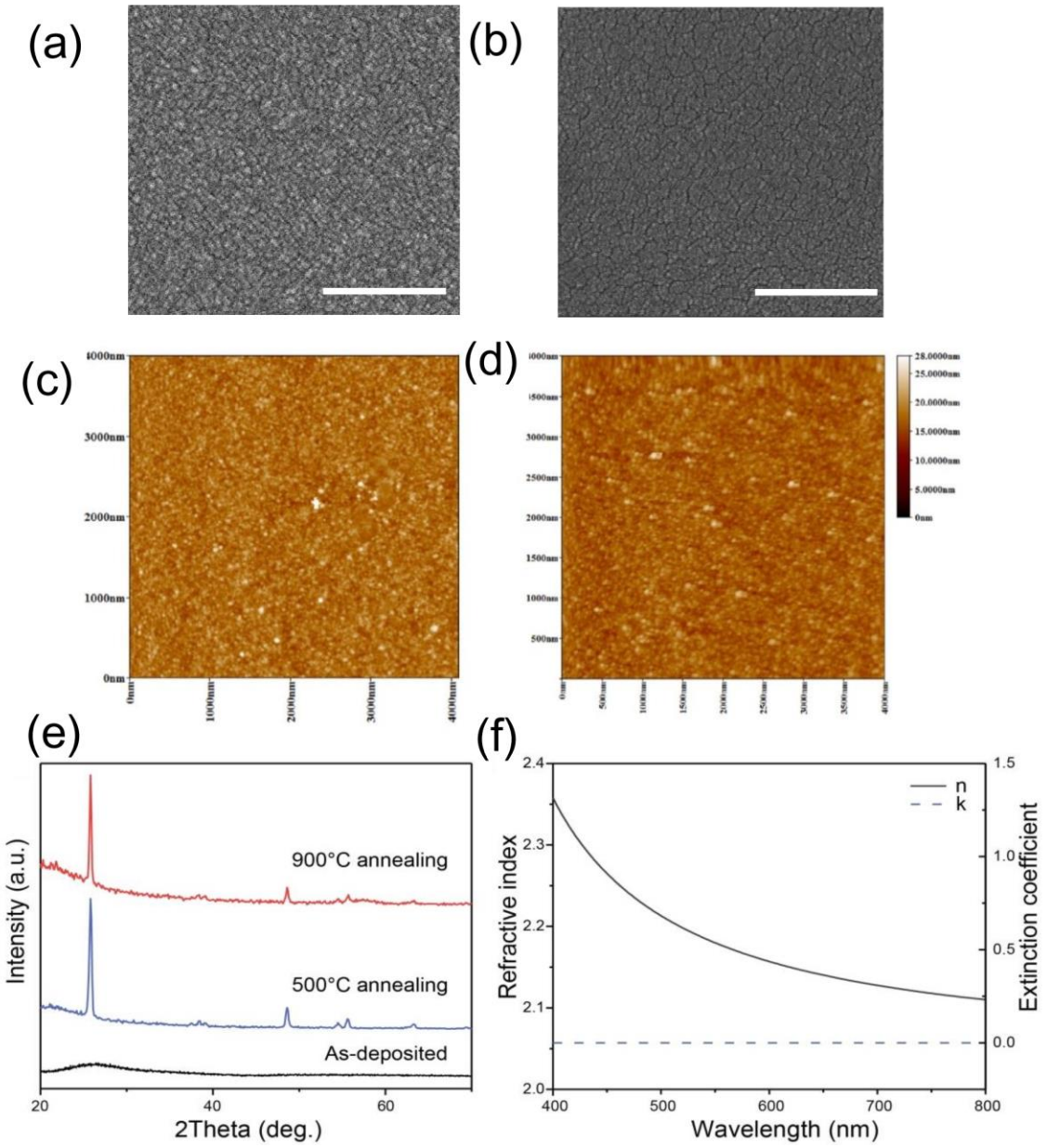

Fig. S1. The deposition and transition of TiO_2 film. (**a** ,**b**) Top view scanning electron microscope (SEM) image of the TiO_2 film before (a) and after (b) 500 °C thermal annealing. The scale bar is 100 nm. (**c**, **d**) AFM images of the TiO_2 film before (c) and after (d) 3 min H^+ implantation. (**e**) The XRD spectrum of the as-deposited and 500 °C, 900 °C annealing TiO_2 film. (**f**) The refractive index and light extinction coefficient of TiO_2 film.

Meanwhile, we have also studied the properties of black TiO_2 with energy dispersive spectrometer (EDS). With the transition from TiO_2 to black TiO_2, more oxygen vacancies generated. Correspondingly, the ratio between Ti and O will also be changed. Figure S2(a) shows the corresponding EDS spectra before and after the H^+ implantation. The molar ratio of oxygen over titanium was 1.76 in as-deposited TiO_2 film. After H^+ implantation, the ratio decreased to 1.25, indicating the generation of oxygen vacancy. This is consistent with the initial expectation and can also indicate the generation of black TiO_2 after the H^+ ion implantation.

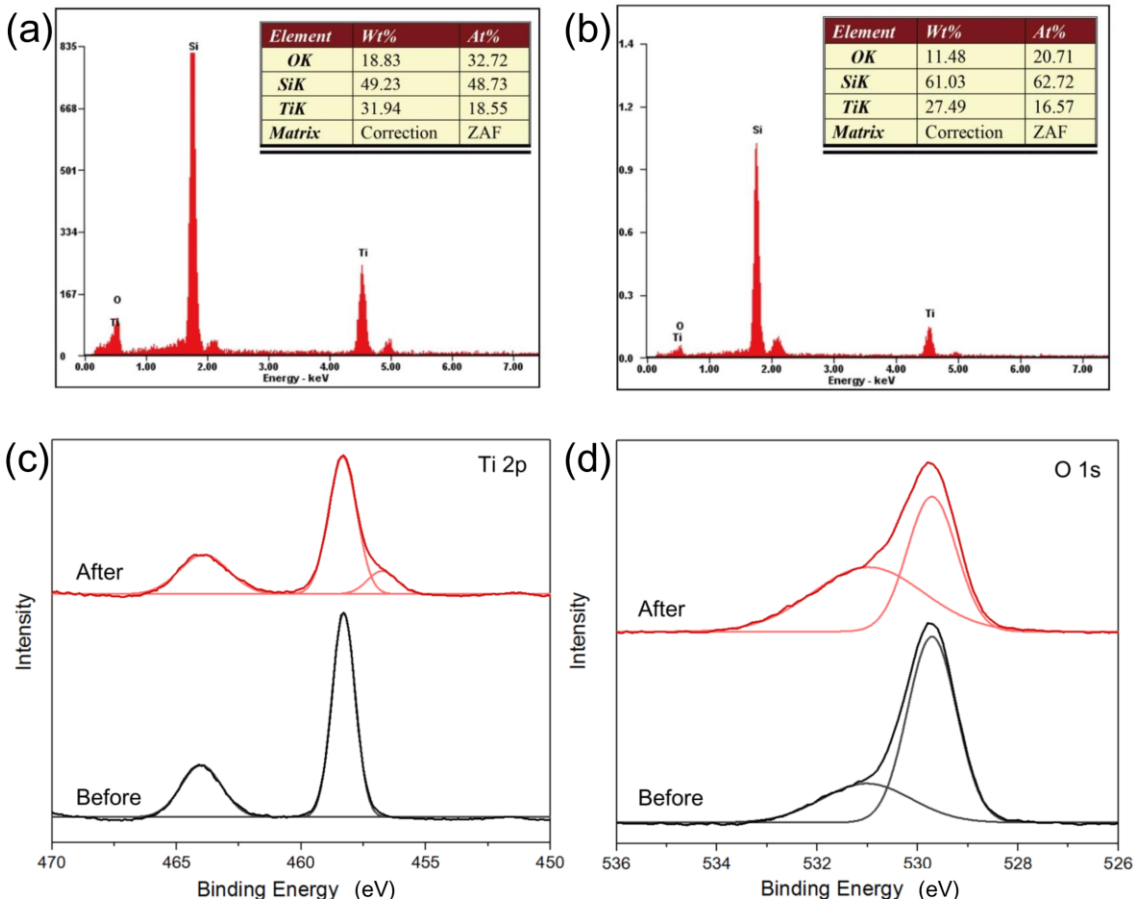

Fig. S2. Fabrication process and characterization of the nanostructures. (**a**, **b**) EDS spectrum of the deposited TiO_2 films (a) before and (b) after H^+ implantation. (c, d) XPS spectra of Ti 2p (**c**) and O 1s (**d**) and their peak deconvolution of the TiO_2 film before and after H^+ implantation.

To further confirm what is responsible for the change in color of TiO_2 film after H^+ implantation, we have performed the XPS measurements. The corresponding results are shown in fig. S2(c) and (d). For the as-deposited TiO_2 film, three dominant peaks have been achieved at 464.0 eV, 458.3 eV, and 529.4 eV. The first two peaks correspond to the Ti 2p peaks (fig. S2(c)). The third one relates to the O 1S (fig. S2(d)). For the as-deposited TiO_2 film, there is a small peak at ~ 530.9 eV. According to the literature (23), this peak corresponds to the oxygen-deficient phase of TiO_{2-x}. It indicates that a small amount of oxygen vacancies have been produced during the E-beam deposition. Once the TiO_2 film is implanted with H^+ ions, significant differences can be

clearly seen. The intensities of peaks at 464.0 eV， 458.3 eV, and 529.4 eV all reduce, whereas the intensity of peak relating to oxygen vacancy at 530.9 eV increases obviously. Meanwhile, the peak at 458.3 eV became broader and it can be resolved into a peak at 458.3 eV and a new peak at ~ 456.7 eV. Following the research in Ref. (24), this new peak is caused by the Ti^{3+} species. The above changes are also consistent with our previous EDS measurements (see fig. S2(a) and (b)). Based on the XPS measurements, we thus can confirm the formation of Ti^{3+} species and oxygen vacancies during the ion implantation.

Section S2. Fabrication process and characterization of the nanostructures

In the method section, we have described the fabrication process of the TiO_2 metasurfaces. Here we show the experimental details with a schematic picture. As shown in fig. S3(a), the TiO_2 metasurfaces were fabricated with electron beam (E-beam) lithography, followed by a lift-off process. The ITO glass substrates were cleaned in ultrasound bath in acetone, isopropyl alcohol (IPA) and DI water for 15 minutes respectively and dried under clean nitrogen flow. Then 350 nm ZEP520 film was spin-coated onto the ITO glass substrates (4000 r/min) and baked at 180 °C on hot plate for 10 minutes. Afterwards, the designed nanostructures were patterned with electron beam in E-beam writer (Raith E-line, 30 kV) and developed in ND510 solution and MIBK at 0 °C for 60 s and 10 s, respectively. The samples were then dried with nitrogen gas before they were transferred into an E-beam evaporator. The E-beam evaporation process is quite similar to the TiO_2 film. The coating process is highly directional and perpendicular to the substrate. As a result, after 200 nm TiO_2 film was deposited onto the substrate, it can be lift-off after immersing the samples in acetone for 8 h, the ZEP patterns were removed and the designed TiO_2 metasurfaces were obtained.

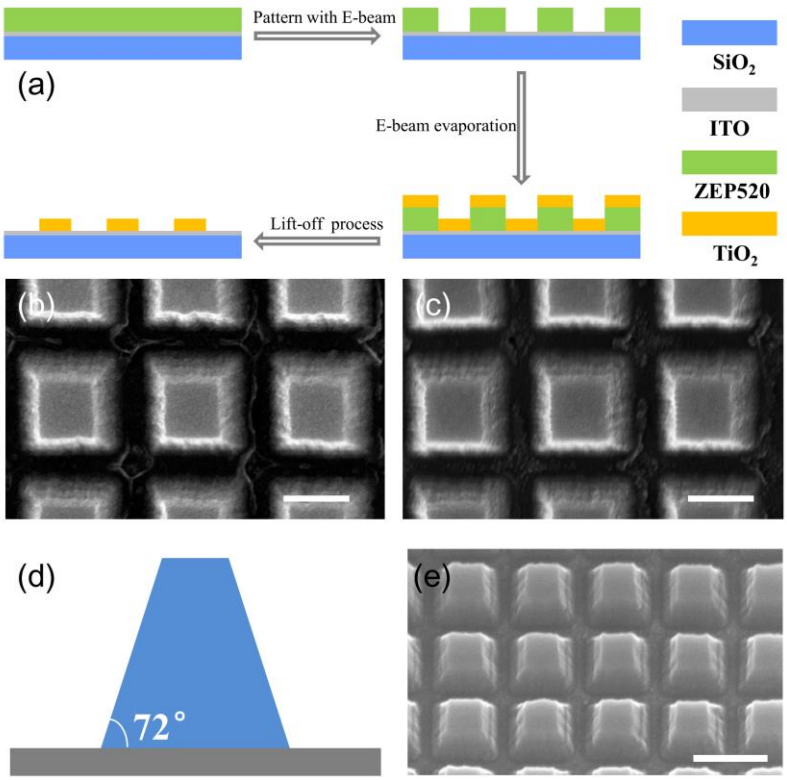

Fig. S3. Numerical calculation and the Mie resonances in TiO_2 metasurfaces. (**a**) Fabrication process of TiO_2 metasurfaces. (**b**, **c**) The SEM images of TiO_2 metasurfaces (l = 330 nm) before (a) and after (b) H^+ implantation. The TiO_2 nanostructures were well preserved during the transition process. The scale bar is 200 nm. (**d**) The cross-section of TiO_2 nanostructure in vertical direction. (**e**) The tile-view SEM image of the metasurface. The trapezoidal angel was fixed at 72°, which was attributed to the lift-off process.

Figure S3(b) shows the top-view SEM image of the final TiO_2 metasurface. The scale bar is 200 nm. We can see that the top surface is as smooth as the film in fig. S1. The sidewall is relatively rough but is still on the order of 10 nm, which is much smaller than the resonant wavelengths. From the top view, we can see that each TiO_2 has square shape, similar to our design well. The bottom squares always larger than the top squares, giving a trapezoid shape in vertical direction. This information can be more clearly seen in vertical cross-section SEM image. As shown in fig. S3(d) and fig. S3(e), the trapezoidal angle is about 72 degree, consistent with our previous experimental result very well.

More than the fabrication of TiO_2 metasurfaces, it is more important to confirm that the transition between TiO_2 and black TiO_2 won't change the nanostructures. This is the basis of this whole research. This information can be more clearly seen from the high-resolution SEM images. As shown in fig. S3(c), both of the TiO_2 nanoblocks (including sizes and trapezoidal angle) and the lattice size are exactly the same the as-fabricated TiO_2 metasurfaces in fig. S3(b). This confirmation is very important for the following numerical designs and the dynamic TiO_2 metasurfaces.

Section S3. Numerical calculation and the Mie resonances in TiO_2 metasurfaces

All the numerical calculation in this work was realized by commercial available finite elements method-based software, COMSOL Multiphysics. Periodic boundary conditions were used in the software to simulate the periodic array of the metasurface with one unit cell. TiO_2 metasurfaces in our work were fabricated on 13 nm ITO glass substrate. The refractive index (n) and extinction coefficient (k) of TiO_2 were measured by spectroscopic ellipsometry.

According to the Mie theory, when illuminated by incident light, sufficiently small spherical dielectric nanoparticles provide both electric- and magnetic type responses of comparable strengths. When the effective wavelength (λ/n) is of the order of the particle diameter (2R), the coupling of incident light and the circular displacement current of the electric field results in the resonant magnetic dipole response. The magnetic resonance that raises from the condition mentioned above may provide a major contribution to the scattering efficiency, and is not associated with large non-radiative loss.

In case of dielectric metasurfaces, the resonances within each nanoparticle play essential roles in tailoring the amplitude and phases of incident light. Owing to its relatively high reflective index, a single TiO_2 nanoparticle can support Mie magnetic (MD) and electric (ED) dipole resonances in the visible spectrum. In case of nanoparticle array, the collective efforts make the reflectance much higher and stronger. In this sense, resonant modes with narrower full width at half maximum (FWHM) and stronger intensity can be generated in the reflection spectrum (see fig. S4(a)). The FWHM of two modes are around 20 nm and the reflectance is close to 100%. Such kind of reflection peaks are good enough to support distinct colors and generate narrow band absorption (when TiO_2 was converted to black TiO_2), whose applications have been experimentally demonstrated in the main text. Figure S4(b) show the corresponding field patterns. The arrows correspond to the direction of electric or magnetic field. When the metasurface was illuminated with an x polarized light, the electric fields are dominated by Ex (X-Z cross-section in ED), and the magnetic field is circulating around x-axis (Y-Z cross section in ED). Simultaneously, the magnetic fields are dominated by Hy (Y-Z cross-section in MD), and the electric field is circulating around y-axis (X-Z cross section in MD). It can be concluded that the mode at the shorter wavelength is induced by the electric dipole, while the longer wavelength mode is the magnetic resonance. This is also consistent with our previous reports.

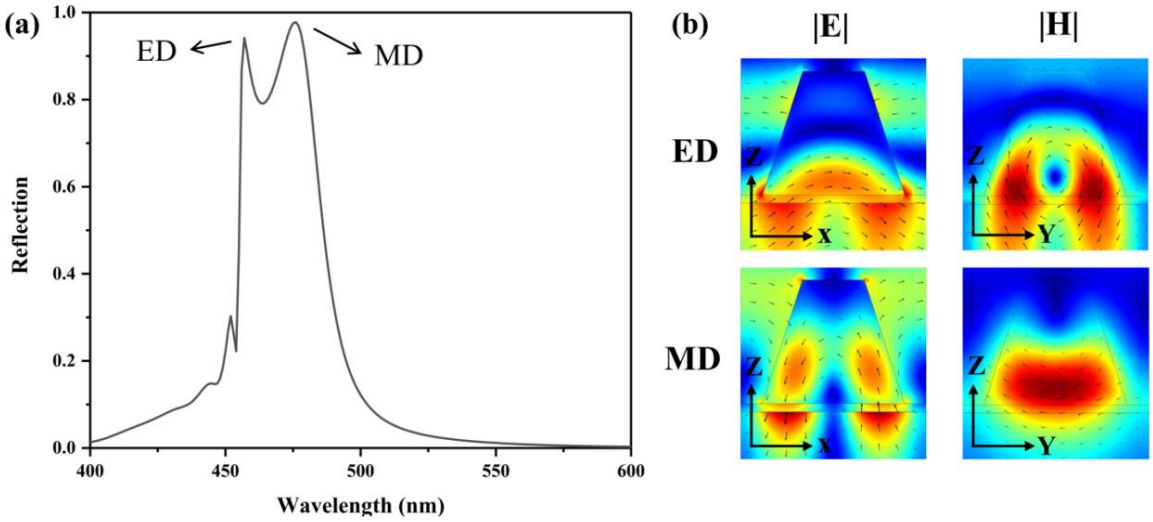

Fig. S4. The numerical simulation of Mie resonance. (**a**) The numerically simulated reflection spectrum of TiO_2 metasurface. (**b**) The electric and magnetic fields of resonances at 457 nm and 478 nm, respectively. According to their field distributions, they are electric (dipole) and magnetic (dipole) resonances, respectively. Here, the period p, nanoblock width w, and thickness t are 300 nm, 230 nm, 200 nm, respectively.

The implantation of H^+ ions will induce the slightly decreasing of refractive index of TiO_2, as shown in main manuscript. We calculated the impact of the n value to the Mie resonance in TiO_2 metasurface. Figure S5(a) shows the reflection spectrum of TiO_2 metasurface (l = 280 nm, p = 350 nm) with n value before and after implantation. The peak position shift was less than 10 nm, with the peak shape almost fixed.

The conditions of black TiO_2 metasurface with lower reflection intensity and weaker electric and magnetic fields were also calculated, and the results were shown in fig. S5(a) and fig. 5S(b). After implantation of H^+ ions for 4 minutes, the intensity of the electric (magnetic) field became extremely weak, indicating that most of the energy of the incident photons was absorbed by the TiO_2, leading to a lower reflection spectra.

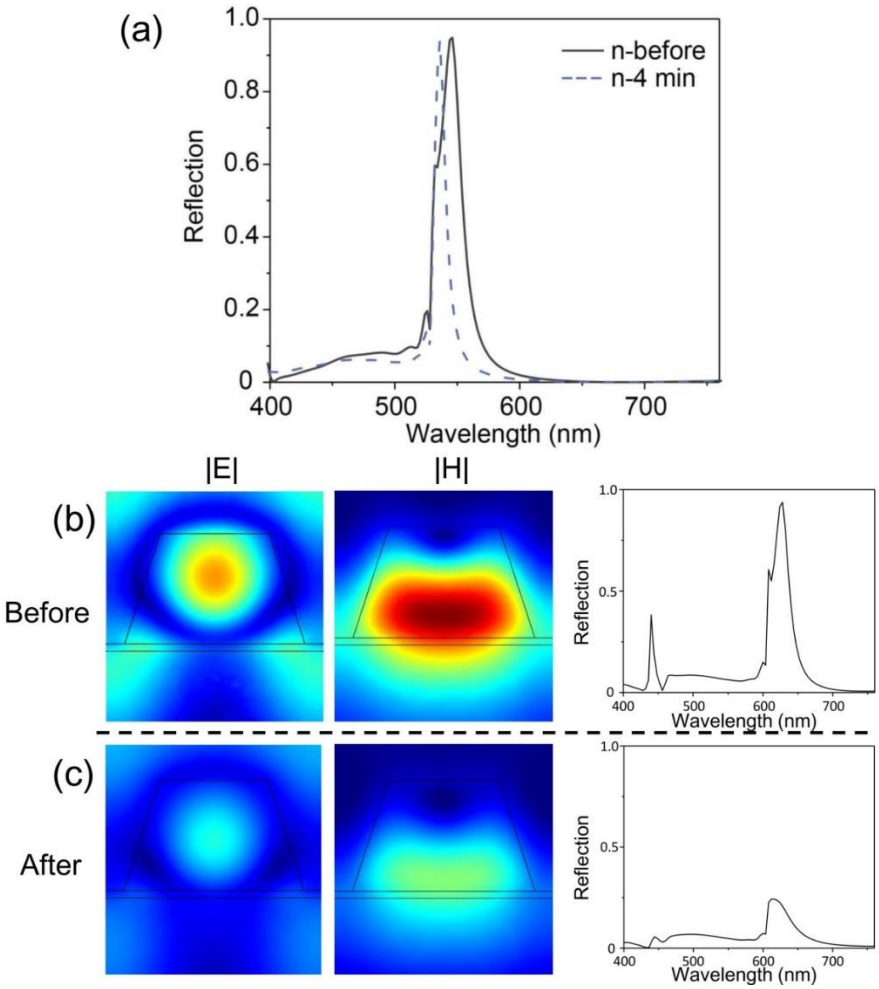

Fig. S5. The numerical simulation of the TiO_2 metasurface before and after H^+ implantation. (**a**) Calculated reflection spectrum of TiO_2 metasurface with the n value before and after H^+ implantation. (**b**, **c**) Numerical calculated field patterns in Z-Y cross-section and reflection spectrum of TiO_2 metasurfaces before (b) and after H^+ implantation (c). Here, the period p, nanoblock width w, and thickness t are 400 nm, 330 nm, 200 nm, respectively. The k value was taken from the spectroscopic ellipsometry measurement results of TiO_2 film after 4 min H^+ implantation.

Section S4. Characterization of TiO_2 metasurfaces

The optical measurements are important for this research. Here we show the experimental details in fig. S6(a). Basically, a white light (Thorlab SLS201L/M, 0.1 mJ/cm^2, 400-800nm) is collimated by an optical lens. Then the white light beam is focused by an objective lens (20X, NA = 0.4) onto the sample surface with nearly normal incidence. The reflected light is collected by the same objective lens and coupled to a CCD camera (Princeton Instrument BUV enhanced CCD) coupled spectrometer (Acton SpectroPro 2750i, f = 750 mm). The transmitted light was collected by another optical lens and coupled to the same spectrometer.

Compared with the transmission (T) and reflection (R) spectra, the absorption spectrum plays a more important role in TiO_2 metasurfaces. For conventional TiO_2 metasurfaces, the low loss

maintains the high efficiencies of meta-devices in the entire visible range. In case of black TiO_2, the resonant enhanced absorption can be used to supply the dip in the absorption spectrum of synthesized black TiO_2. It can also be used to selectively absorb light with particular wavelengths. Due to the presence of scattering and diffraction, the absorption cannot be directly obtained with the simple equation A = 1-T-R. In our experiment, the absorption curve is achieved with two steps (see fig. S6(b)). We firstly measured the transmission (T_1) and reflection (R_1) spectra of white TiO_2 metasurfaces. As the material itself has negligibly small absorption, the scattering and diffraction of TiO_2 nanostructures can be obtained with $D = 1-T_1-R_1$. When the TiO_2 was converted to black TiO_2, according to the results in main manuscript, the real parts of refractive index changed very small. As a result, the scattering and diffraction of the nanostructures should be preserved. After measuring the transmission (T_2) and reflection (R_2) spectra of black TiO_2 metasurfaces, the absorption of black TiO_2 metasurface can thus be expressed as $A = 1-D-T_2-R_2$.

Based on the above process, we have experimentally fabricated three metasurfaces covering blue, green, and red regions (see top row in fig. S6(c)). After implanting H^+ for 1 minute, the absorption at the corresponding resonant positions is significantly enhanced. As a result, the controllable narrowband absorption can be achieved with this method (see bottom row in fig. S6(c)).

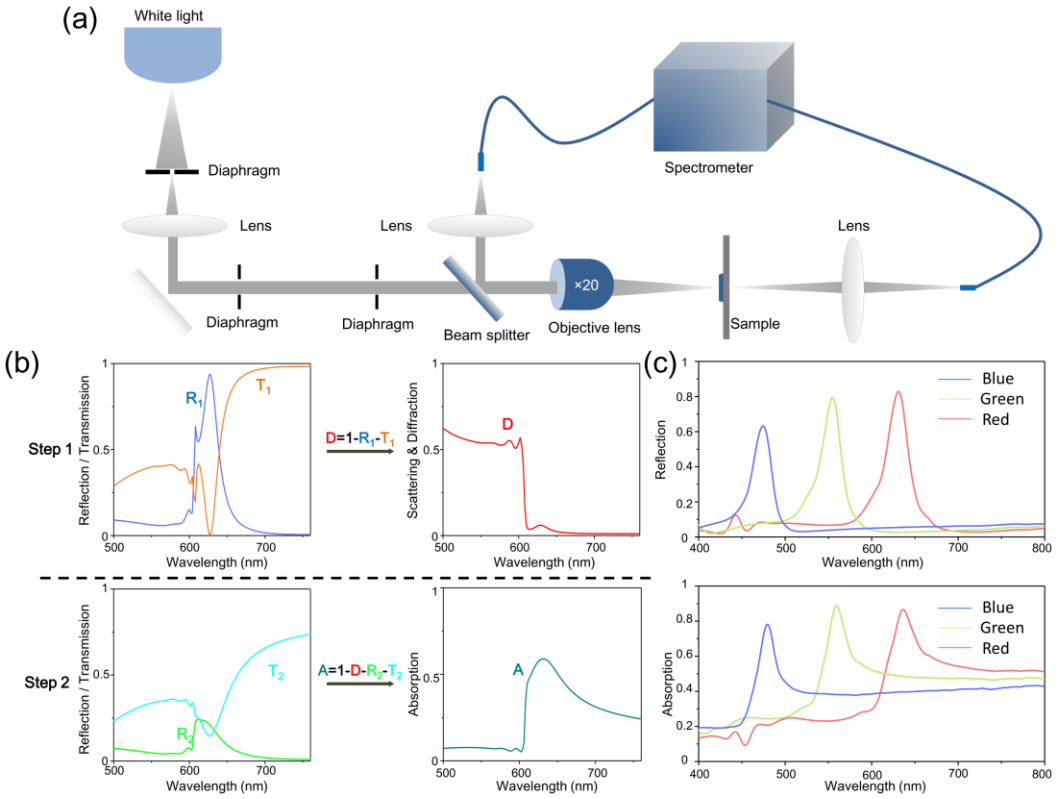

Fig. S6. Optical measurement of TiO_2 metasurfaces. (**a**) The experiment setup for optical characterization. (**b**) The schematic process to obtain the absorption process. Here the structural parameters of TiO_2 metasurface are l = 400 nm, w = 330 nm. (**c**) The reflection spectra of conventional TiO_2 metasurfaces (top row) and the corresponding absorption spectra of black TiO_2 metasurfaces (bottom row). Here the structural parameters of three metasurfaces are p = 300 nm, w = 230 nm for blue, p = 350 nm, w = 280 nm for green, and p = 400 nm, w = 330 nm for red.

Section S5. Dynamic image in TiO_2 metasurfaces

The transition between TiO_2 and black TiO_2 is important for practical applications. For dynamic image, the duality of TiO_2 metasurface is essential. In the main text, we have tested more than 20 transition rounds and the reflectance was well kept. Here we show the corresponding colors in fig. S7(a). Similar to the reflection spectra, the recorded bright-field colors are also well preserved from beginning to 20 times TiO_2-black TiO_2-TiO_2 transition rounds. Since the transition process to black TiO_2 is very tender, we believe this duration time can be much better.

In fig. S7(b), we list the reflection spectrums of 15 samples shown in Fig. 3(d) that before and after H^+ implantation. From the reflection spectrums, we can see that the structural colors of TiO_2 metasurfaces with different sizes span the whole visible spectrum. Moreover, after implantation with H^+ ions, the reflectance became very low, and the corresponding positions on CIE 1931 map shown in Fig. 3(d) of main manuscript shifted to the center as well.

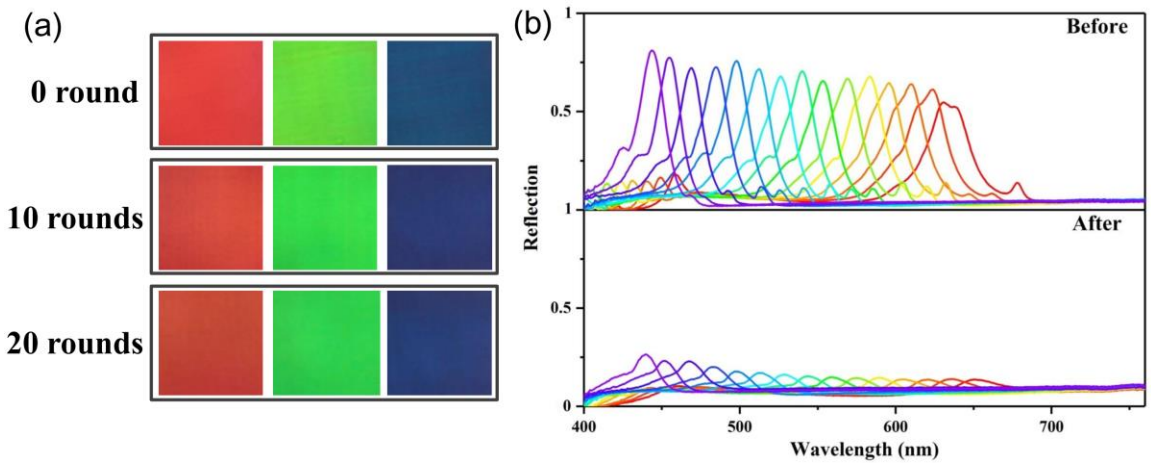

Fig. S7. The color and reflection spectrum of TiO_2 metasurfaces. (**a**) The corresponding structural colors of three metasurfaces in Fig. 4 in the main text. We can see that the structural colors are also well kept after the transition process. (**b**) The reflection spectrums of 15 total TiO_2 metasurfaces with different lattice sizes before and after H^+ implantation.

In the main manuscript, we show that encoded information can be simply concealed after the transition from TiO_2 metasurface to black TiO_2 metasurface. It is important to note that similar efforts have been demonstrated in other material systems. However, in most of these researches, the structural parameters of information and background are quite different. As a result, even though the information cannot be seen under microscope, it is quite easy to be got by directly measuring it with scanning electron microscope (SEM). In contrast to the previous studies, we selected two types of metasurfaces with very similar structural sizes. As a result, the encoded information can only be seen under optical microscope before H^+ implantation (see Fig. 3 in main text). After the transition to black TiO_2 metasurface, the encoded information is concealed. Most importantly, this information is also hard to see in SEM image. Figure S8 shows the same top view SEM image as Fig. 3 in the main text. However, without the guiding lines, the information “COLOR” cannot be observed. This can further improve the applications of TiO_2 metasurfaces in optical encryption and anti-counterfeiting et al.

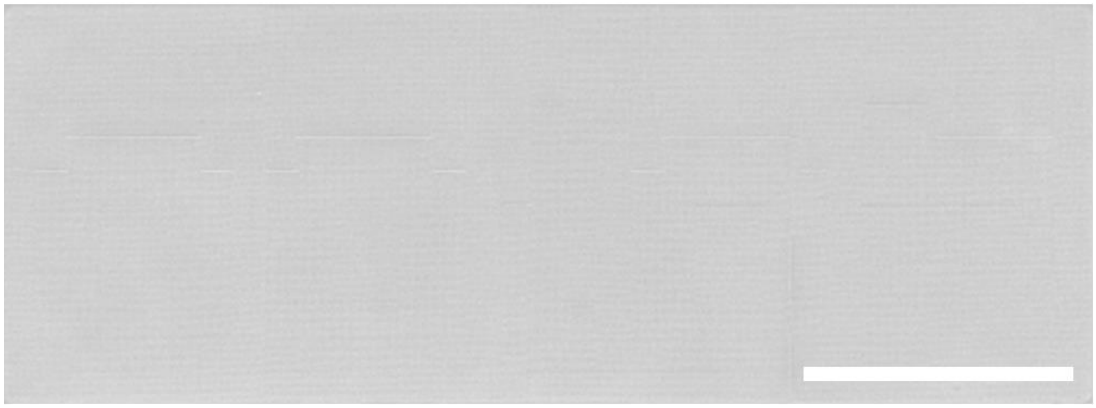

Fig. S8. The SEM image of "COLOR" pattern without guide lines. The SEM image of "COLOR" pattern in Fig. 5(a) without guideline. Because of the similar structure sizes between the letters and background, once the information was encoded by H^+ implantation, it was hard to be identified even in SEM, making the optical encryption more reliable.

Section S6. The photoreduction with TiO_2 metasurfaces

Although newly developing in metasurface field, TiO_2 has been studied in photocatalysis, including water splitting, degradation of organic pollutants and fixation of molecular nitrogen, for several decades. TiO_2 can absorb photons with energy above the bandgap and generate the excited electrons and holes. However, due to the relatively high bandgap (~3.2 eV), only ultraviolet (UV) light (wavelength < 387 nm) can be absorbed by TiO_2. Solar light contains only 2-3% UV light, which enormously limits the development of TiO_2 photocatalysis. As mentioned above, black TiO_2 can reduce the bandgap and absorb the whole visible light. What's more, by fabricating black TiO_2 to nanostructures with subwavelength sizes and engineering the arrangement and geometry of the building blocks of metasurface, we can achieve high absorption or reflection of a certain wavelength of light. In this work, we designed the enhanced absorption wavelength to around 450 nm to further increase the absorption in visible spectra of black TiO_2.

The reaction of photoreduction of $AgNO_3$ to Ag nanoparticles was utilized to demonstrate the enhancing absorption of TiO_2 metasurface. All the $AgNO_3$ solution we used in this work is 0.25mol/L. First, the sample was immersed in $AgNO_3$ solutions and illuminated with white light or single-wavelength laser. The schematic of experimental setup was show in fig. S9(a). After illumination, the sample was rinsed with deionized water and then blown dry with a nitrogen gun. Then the sizes of Ag nanoparticles generated on the surface of TiO_2 metasurfaces or films were characterized by SEM. Notably, to eliminate the effect of immersing time, all the samples were immersed in $AgNO_3$ solution for 60s, and the only difference is the illuminating time.

The resonance wavelength of the metasurface is strongly influenced by the refractive index (n) of the environment media. We have measured the reflection spectrum of TiO_2 metasurface before and after immersed into the $AgNO_3$ solution and the results are shown in fig. S9(b). The absorption spectrum of black TiO_2 metasurface mentioned in Fig. 5 of the manuscript was also shown in fig. S9(c)

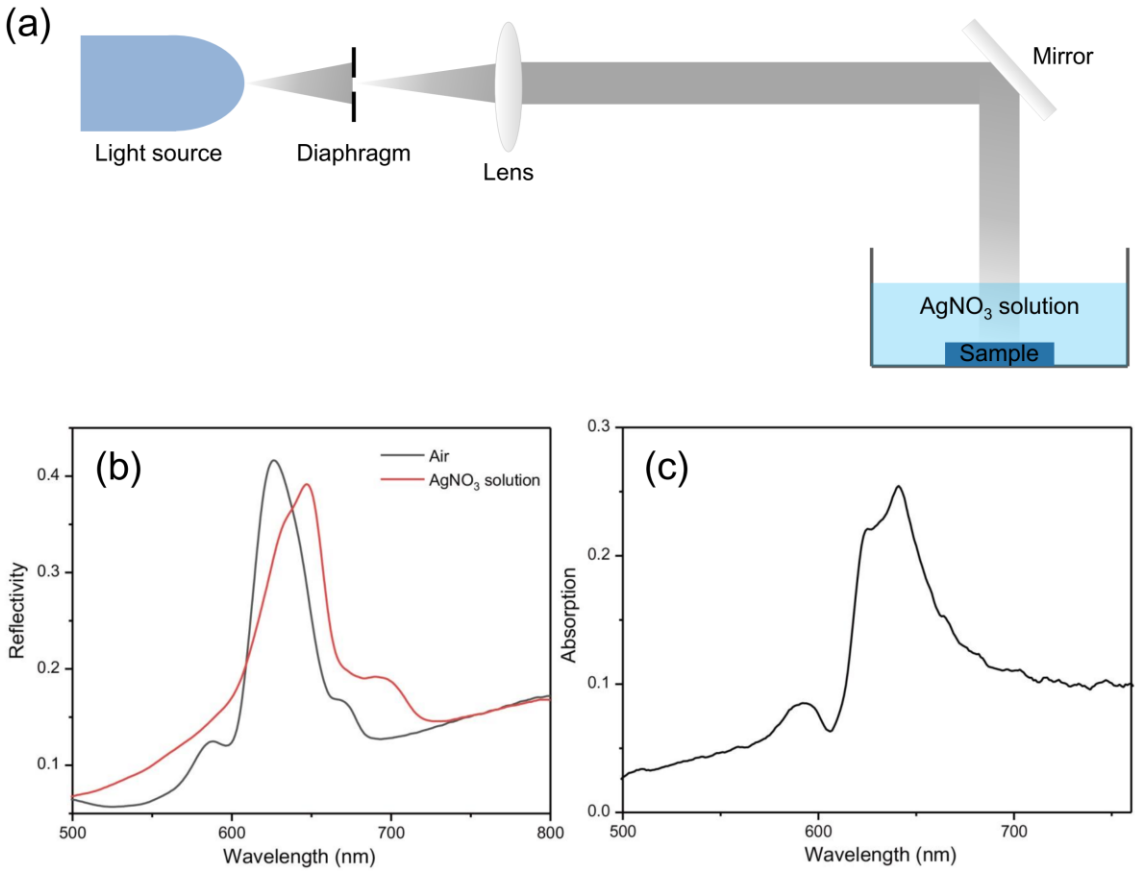

Fig. S9. Setup for photoreduction and the characterization of the TiO_2 metasurface in $AgNO_3$ solution. (**a**) The setup for photoreduction of Ag nanoparticles. (**b**) Reflection spectrum of TiO_2 metasurface in air and immersed in $AgNO_3$ solution. (**c**) The absorption spectra of black metasurface in Fig. 5 of the manuscript.

We have performed an additional experiment by immersing an ITO glass (thickness of ITO is 13 nm) in $AgNO_3$ solution with white light illuminating for 60s (The longest exposure time used in the manuscript) and observed the surface by SEM (fig. S10(a) and (b)). We found that after illuminating, there was no obvious silver nanoparticle generated on the ITO surface. Although $AgNO_3$ is unstable under light irradiation, the low illuminating intensity and short illuminating time in our experiment was not enough to support the Ag^+ reduction process without any TiO_2.

The generated Ag nanoparticles in our photo-reduction experiments were characterized by transmission electron microscope (TEM, JEM-3200FS). The metasurface after immersed in $AgNO_3$ solution and illuminated with white light was ultrasonic cleaned in ethanol for 5 hours so that the Ag nanoparticles were dispersed in ethanol uniformly. Afterwards, the ethanol dispersed with Ag nanoparticles was dropwised to carbon-coated copper grids to get the TEM sample. Figure S10(c) shows the high-resolution transmission electron microscope (HRTEM), which indicates the high crystallization of Ag nanoparticles and shows clear fringes perpendicular to the edge with a spacing of ca. 0.251 nm that corresponds to {004} reflections of hexagonal crystal system. The inset is selected area electron diffraction (SAED) pattern, which suggested that the as-formed Ag nanostructures were highly pure.

To confirm the effects of black TiO_2 metasurface, two control experiments with regular TiO_2 metasurface and black TiO_2 film have also been performed with the same conditions. By immersing regular TiO_2 metasurface into $AgNO_3$ solution and illuminating with white light, the displayed colors were well kept and no additional nanoparticles have been generated (fig. S10(d)). The black TiO_2 film indeed produced some additional Ag nanoparticles (fig. S10(e)). However, the particle sizes were much smaller than the ones on black TiO_2 metasurfaces (see fig. S10(f)). The two control experiments have also been plotted as dashed line and dash-dotted line in Fig. 4(e) in the manuscript.

In order to confirm the enhancement of photocatalysis performance of the TiO_2 metasurfaces, black TiO_2 film and metasurface were immersed in $AgNO_3$ solution and illuminated with white light for 60s and the nanoparticle generated on them were characterized by SEM. The sizes of Ag nanoparticles on TiO_2 film were far less than that on TiO_2 metasurfaces, as shown in fig. S10(f) and fig. S10(g). The generation of Ag nanoparticles on black TiO_2 film was induced by the photo-decomposition of $AgNO_3$ and weak photo-reduction effect of black TiO_2 film. But the reaction intensity was much weaker than the photo-reduction process dominating by TiO_2 metasurfaces because of the resonance enhanced absorption of metasurface, thus leads to larger Ag nanoparticles.

Moreover, we conducted a contrast experiment that immersed the same two black TiO_2 metasurfaces in $AgNO_3$ solution and illuminated them with white light without or with a UV filter lens (fig. S10(h) and (i)). There is no significant difference in the shapes, particle size of generated Ag nanoparticles between with or without the UV filter lens. This result illustrated that the UV light play little effect on the photo-chemical process of black TiO_2 metasurface.

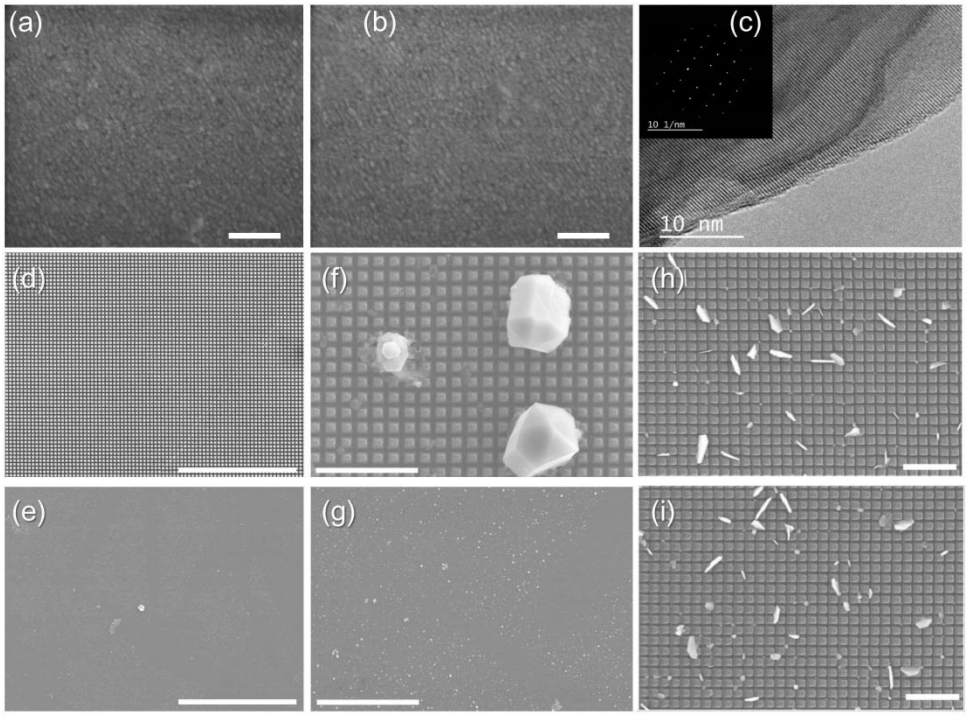

Fig. S10. The contrast experiment of Ag photoreduction and characterization of the generated Ag nanoparticle. (**a**, **b**) The SEM image of the surface of ITO glass with (a) and without (b) immersing in $AgNO_3$ solution and illuminating with white light for 60s (The scale-bar is 200 nm). (**c**) The high-resolution transmission electron microscope (HRTEM) images. The inset is the selected area electron diffraction (SAED) pattern. The scale bar is 2 nm. (**d**, **e**) The SEM images of control experiment with (d) conventional TiO_2 metasurface and (e) black TiO_2 film after immersing in $AgNO_3$ solution and illuminating with white light for 60s. The scale bar is 10 μm. (**f**, **g**) The SEM images of black TiO_2 film (f) and metasurface (g) after immersing in $AgNO_3$ solutions and illuminating for 60s. The scale bar is 2μm. (**h**, **i**) The SEM image of black TiO_2 metasurface after immersing and illuminating process without and with UV filter lens. The scale bar is 2 μm.

As shown in fig. S11(a), when the black TiO_2 metasurface was immersed in $AgNO_3$ solution for 60s without illuminating, the particle sizes of the majority of the generated Ag nanoparticles were less than 0.5 μm. With the illuminating time increase from 0s to 20s, 40s and 60s, the particle-size distributions gradually move to the right side. When the sample was illuminated for 60s, the nanoparticles grow to 1~2 μm, and the largest one was greater than 2.5 μm.

The SEM images of wavelength dependent photo-reduction experiment were shown in fig S11(b-i), and the relationship between the mean particle sizes of newly generated Ag nanoparticles and the laser wavelength was shown in Fig. 5 in the manuscript.

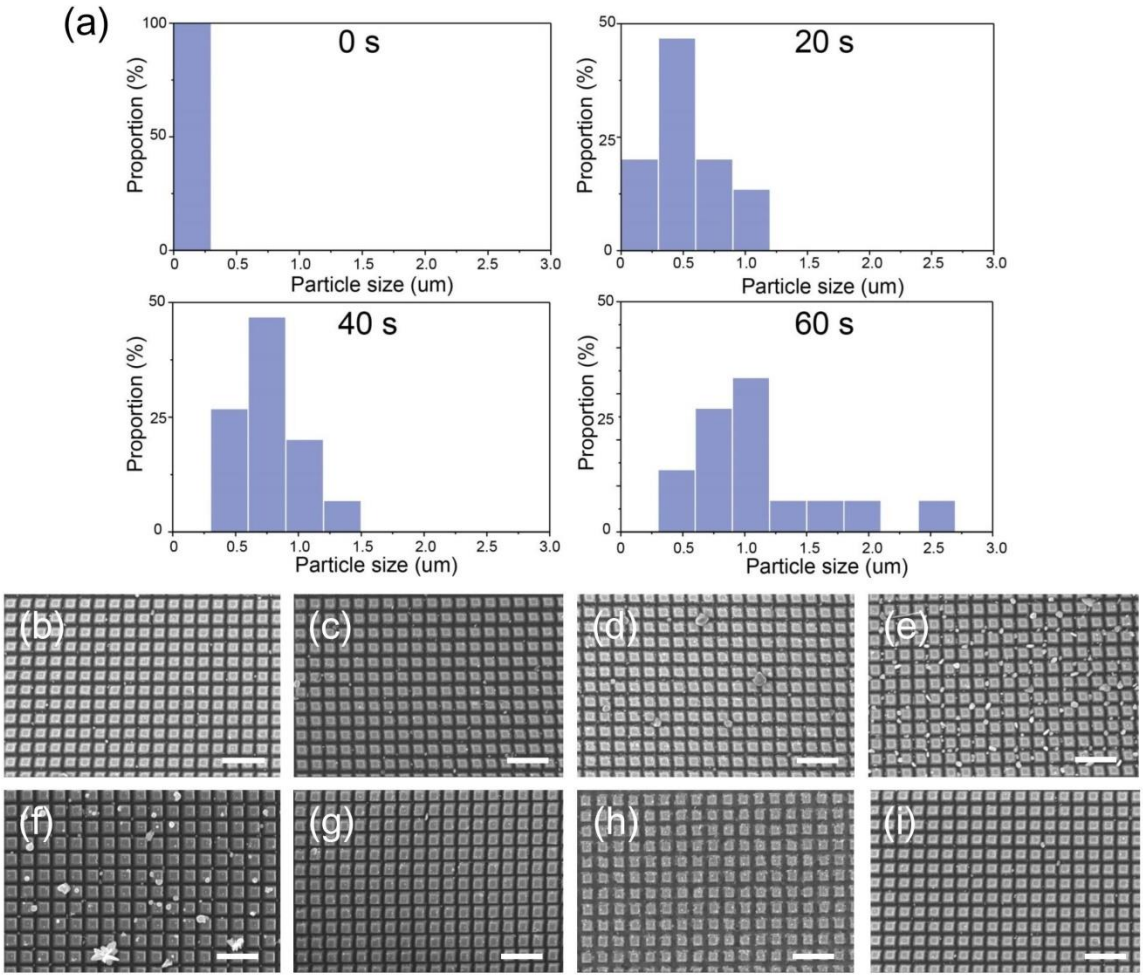

Fig. S11. Characterization of particle sizes of Ag photoreduction on TiO_2 metasurfaces. (**a**) Particle-size distributions of the Ag nanoparticles on black TiO_2 metasurfaces with different illuminating time shown in Fig. 4. (**b**-**i**) The SEM images of black TiO_2 metasurfaces after immersed in $AgNO_3$ solutions and illuminated with lasers of (b) 600 nm, (c) 620 nm, (d) 625 nm, (e) 630 nm, (f) 640 nm, (g) 650 nm, (h) 680 nm, (i) 700 nm, respectively. The scale bars are all 1 μm.